Enzyme Catalysis and Regulation:

Comparative Analysis of Two UDP-glucose Dehydrogenases in *Pseudomonas aeruginosa* PAO1

Ruei-Jiun Hung, Han-Sheng Chien, Ruei-Zeng Lin, Ching-Ting Lin, Jaya Vatsyayan, Hwei-Ling Peng and Hwan-You Chang

J. Biol. Chem. 2007, 282:17738-17748.
doi: 10.1074/jbc.M701824200 originally published online April 18, 2007

THE JOURNAL OF BIOLOGICAL CHEMISTRY VOL. 282, NO. 24, pp. 17738–17748, June 15, 2007

Comparative Analysis of Two UDP-glucose Dehydrogenases in *Pseudomonas aeruginosa* PAO1*[S]

Received for publication, March 1, 2007, and in revised form, April 17, 2007 Published, JBC Papers in Press, April 18, 2007, DOI 10.1074/jbc.M701824200

Ruei-Jiun Hung[‡], Han-Sheng Chien[‡], Ruei-Zeng Lin[‡], Ching-Ting Lin[§], Jaya Vatsyayan[‡], Hwei-Ling Peng[§], and Hwan-You Chang[‡1]

From the [‡]Institute of Molecular Medicine, National Tsing Hua University and the [§]Department of Biological Science and Technology, National Chiao Tung University, Hsin Chu 300, Taiwan, Republic of China

UDP-glucose dehydrogenase (UGDH) catalyzes a two-step NAD^+-dependent oxidation of UDP-glucose to produce UDP-glucuronic acid, which is a common substrate for the biosynthesis of exopolysaccharide. Searching the *Pseudomonas aeruginosa* PAO1 genome data base for a UGDH has helped identify two open reading frames, *PA2022* and *PA3559*, which may encode a UGDH. To elucidate their enzymatic identity, the two genes were cloned and overexpressed in *Escherichia coli*, and the recombinant proteins were purified. Both the gene products are active as dimers and are capable of utilizing UDP-glucose as a substrate to generate UDP-glucuronic acid. The K_m values of PA2022 and PA3559 for UDP-glucose are ~0.1 and 0.4 mM, whereas the K_m values for NAD^+ are 0.5 and 2.0 mM, respectively. Compared with PA3559, PA2022 exhibits broader substrate specificity, utilizing TDP-glucose and UDP-*N*-acetylglucosamine with one-third the velocity of that with UDP-glucose. The *PA2022* mutant and *PA2022-PA3559* double mutant, but not the *PA3559* mutant, are more susceptible to chloramphenicol, cefotaxime, and ampicillin. The *PA3559* mutant, however, shows a reduced resistance to polymyxin B compared with wild type PAO1. Finally, real time PCR analysis indicates that *PA3559* is expressed primarily in low concentrations of Mg^{2+}, which contrasts with the constitutive expression of *PA2022*. Although both the enzymes catalyze the same reaction, their enzymatic properties and gene expression profiles indicate that they play distinct physiological roles in *P. aeruginosa*, as reflected by different phenotypes displayed by the mutants.

UDP-glucose dehydrogenase (UGDH)[2] (EC 1.1.1.22) converts UDP-glucose (UDP-Glc) to UDP-glucuronic acid (UDP-GlcUA) accompanied by the reduction of two molecules of NAD^+. The importance of UDP-GlcUA is readily apparent considering the downstream polymers that utilize this compound or its descendents, such as UDP-xylose, UDP-arabinose, and UDP-galacturonic acid (1). The cellular functions of UGDH have been investigated in a number of organisms, and these studies demonstrate its importance in detoxification, polysaccharide biosynthesis, and embryonic development (2). In the liver, glucuronide conjugation of xeno- and endobiotic compounds by UDP-glucuronosyltransferases is an important way to aid in solubilizing these metabolites (3). In plants, both UDP-GlcUA and its derivative, UDP-xylose, are essential to synthesizing cell wall polysaccharides such as hemicellulose (4). Animals require UDP-GlcUA to synthesize major structural polysaccharides such as hyaluronic acid (HA), heparan sulfate, and chondroitin sulfate (5). An inability to synthesize these structural polysaccharides may partly explain why a UGDH deficiency disrupts the *Wingless* signal pathway in *Drosophila melanogaster* (6–8) and arrests mesoderm and endoderm migration during gastrulation in mice (9).

In many pathogenic bacteria, UDP-GlcUA is necessary for the synthesis of exo- polysaccharides (EPS) and lipopolysaccharides (LPS). The formation of these polysaccharides is critical to bacterial virulence (10, 11) because it enables the bacteria to evade attacks by a host immune system, such as phagocytosis (12, 13). Some pathogens, including group A and C streptococci, can even synthesize nonimmunogenic EPS such as HA to prevent antibody-mediated killing (14). Recent studies demonstrate that UGDH mutation in the pathogenic fungus *Cryptococcus neoformans* alters the cell integrity and nucleotide sugar pool. The cells also become temperature-sensitive and fail to grow in an animal model (15).

Pseudomonas aeruginosa, a Gram-negative bacterium, is noted for its environmental versatility, resistance to antibiotics, and ability to cause life-threatening infections in cystic fibrosis, burn, and immunocompromised patients (16). Epidemiological data indicate that *P. aeruginosa* is the third leading cause of nosocomial infection (17). The significance of EPS in *P. aeruginosa* virulence is well documented in the cystic fibrosis strains, in which the synthesis of a large quantity of alginate has frequently been observed. However, many other pathogenic *P. aeruginosa* strains, such as PAO1, do not normally produce alginate. The precise structure and composition of the EPS and the genes required for EPS synthesis in these *P. aeruginosa* strains remain unclear. Because UDP-GlcUA is one of the most commonly found sugar donors for bacterial EPS synthesis, this

* This work was supported by the National Science Council and the National Research Program of Genome Medicine, Taiwan. The costs of publication of this article were defrayed in part by the payment of page charges. This article must therefore be hereby marked "*advertisement*" in accordance with 18 U.S.C. Section 1734 solely to indicate this fact.

[S] The on-line version of this article (available at http://www.jbc.org) contains supplemental Figs. S1–S3.

[1] To whom correspondence should be addressed: Institute of Molecular Medicine, National Tsing Hua University, 101 Kuang Fu Rd., 2nd Sec., Hsin Chu 300, Taiwan. Tel.: 886-35742909; Fax: 886-35742910; E-mail: hychang@life.nthu.edu.tw.

[2] The abbreviations used are: UGDH, UDP-glucose dehydrogenase; UDP-GlcUA, UDP-glucuronic acid; DTT, dithiothreitol; G3PDH, glyceraldehyde-3-phosphate dehydrogenase; HA, hyaluronic acid; HPLC, high pressure liquid chromatography; MIC, minimal inhibition concentration; LPS, lipopolysaccharide; EPS, of exo-polysaccharide; GMDH, GDP-Man dehydrogenase.

TABLE 1
Bacterial strains and plasmids used in this study

Strain or plasmid	Genotype or relevant characteristic	Source or Ref.
P. aeruginosa		
PAO1	Wild type	39
RJ101	PAO1 ΔPA2022	This study
RJ102	PAO1 ΔPA3559	This study
RJ103	PAO1 ΔPA2022 ΔPA3559	This study
E. coli		
NovaBlue (DE3)	*endA1 hsdR17 supE44 thi-1 recA1 gyrA96 relA1 lac* [F′ *proAB lacI*^{q}ZΔM15 Tn*10*] (DE3)	Novagen
Top10	F$^-$ *mcrA* Δ(*mrr-hsdRMS-mcrBC*) φ80*lacZ*ΔM15 Δ*lacX*74 *deoR nupG recA*1 *araD*139 Δ(*ara-leu*)7697 *galU galK rpsL*(Str^R) *endA1*	Invitrogen
S17–1 λpir	Tp^r Sm^r *recA*, *thi*, *pro*, *hsd*R$^-$M$^+$ RP4: 2-Tc:Mu: Km Tn*7* λ*pir*	40
SM10 λpir	Km^r, *thi-1*, *thr*, *leu*, *tonA*, *lacY*, *supE*, *recA*::RP4–2-Tc::Mu, *pir*	40
Plasmids		
pET-30a	His-tagged protein expression vector, Km^r	Novagen
pSUP202	Cm^r Tc^r Ap^r Mob$^+$	40
pEX18Tc	Gene-replacement vector; *sacB*$^+$, *oriT*$^+$ Tc^r	31
pHC727	A 1.4-kb fragment containing PA2022 cloned into pET30a	Laboratory stock
pRJ001	A 1.5-kb BamHI-XhoI fragment containing PA3559 cloned into pET30a	This study
pRJ002	PA3559 knockout construct in pEX18Tc, Tc^r	This study

TABLE 2
Oligonucleotides used in this study

Primer	Description	Sequence (5′ → 3′)
RJ004	PA3559 overexpression	AGGGGATCCCCATGAAGATCAGCGTATTCGGCAGTGGC
RJ003	PA3559 overexpression	TTACTCGAGTCAGGCCTGGCGCAACAGGCG
HY1001	PA2022 overexpression	CTCATATGCGGCTATGCGTGATTGGT
HY1002	PA2022 overexpression	GGCTGCGCTCGCCTTACAATG
pmrE05	PA3559 upstream region cloning	GGCGCCTGCGTCGTAGCGA
pmrE03	PA3559 upstream region cloning	TTTCCTCGACGGAGGATCCGC
pmrE04	PA3559 downstream region cloning	GCCACGGATCCCACTACTAC
pmrE06	PA3559 downstream region cloning	TTCATCTGCAGGATAGTCGC
RJ010	G3PDH, forward	ACTATCCGCCTGGCCATCAA
RJ011	G3PDH, reverse	CTTTCGGCATCGTGCTCGAC
RJ014	PA3559 detection, forward	GGCTCTATGGCCACGACGAA
RJ015	PA3559 detection, reverse	ATCGGGTAGTAGTGGAAGCCGTG
RJ020	PA2022 detection, forward	CTACGGCGGCTCGTGCTT
RJ021	PA2022 detection, reverse	CGTCGGTACCCGGCTTGA

study attempts to identify the UGDH encoding gene in *P. aeruginosa* PAO1 and to investigate the biochemistry and functional roles of this enzyme in this important pathogen. This study first demonstrates that at least two *P. aeruginosa* genes can encode a product with UGDH activity, each with a distinct expression pattern and enzyme kinetic parameters. The presence of two types of UGDH motivated the construction of deletion mutants for each of the genes, and this study analyzes and reports on the functional roles of these genes in several biological properties of *P. aeruginosa* PAO1.

EXPERIMENTAL PROCEDURES

Bacterial Strains and Growth Conditions, Plasmids, Oligonucleotide Primers, and Chemicals—Table 1 lists the bacterial strains and plasmids used in this study. *Escherichia coli* and *P. aeruginosa* were cultured in standard Luria-Bertani broth (LB: 10 g/liter tryptone, 5 g/liter yeast extract, 10 g/liter sodium chloride) or on LB agar. The basal medium employed in the determination of minimal inhibition concentration (MIC) of antibiotics and in RNA extraction for quantitative PCR contained 30 mM glucose, 40 mM K_2HPO_4, 22 mM KH_2PO_4, 7 mM $(NH_4)_2SO_4$, and either 2.0 or 0.02 mM $MgSO_4$ for Mg^{2+}-sufficient or Mg^{2+}-deficient conditions, respectively. The following antibiotic concentrations were used to select recombinant *E. coli*: tetracycline, 10 μg/ml; ampicillin, 100 μg/ml; kanamycin, 25 μg/ml. The concentration of tetracycline for selecting recombinant *P. aeruginosa* was 50 μg/ml. Unless indicated otherwise, all chemicals were obtained from Sigma and were of the highest purity available. Table 2 lists the oligonucleotide primers used in this study.

Recombinant DNA Manipulation—Recombinant DNA experiments were carried out by standard procedures as described (18). Restriction endonucleases and DNA-modifying enzymes were purchased from either New England Biolabs (Beverly, MA) or MBI Fermentas (Hanover, MD) and were used according to supplier recommendations. The *PA2022* and *PA3559* overexpression clones were constructed using PCR amplification of the coding region of each respective gene. Specific primer sets and PAO1 genomic DNA served as the template in the reaction. The nucleotide sequence of *PA3559* and *PA2022* was retrieved from the *Pseudomonas* Genome Project. The forward and reverse primers for *PA2022* were HY1001 and HY1002, and those for *PA3559* were RJ004 and RJ003, containing BamHI and XhoI restriction endonuclease sites, respectively. The PCR product was cloned into the pET30a expression vector at corresponding restriction sites to be in-frame with the His_6 tag at the N terminus of the protein. The constructs were then introduced into *E. coli* NovaBlue (DE3) by the rubidium chloride method, and the transformants were selected on LB agar containing 25 μg/ml kanamycin. The DNA was sequenced to verify the correctness of the cloned gene and the reading frame fusion with the His_6 tag.

Overexpression and Purification of His$_6$-tagged PA2022 and PA3559 Products—The production of PA2022 and PA3559 in *E. coli* was carried out by growing the recombinant strains in LB broth supplemented with 25 μg/ml kanamycin and 10 μg/ml tetracycline. The cells were first cultivated by shaking at 37 °C until the A_{600} = 0.5. Isopropyl thio-β-D-galactopyranoside was subsequently added at a final concentration of 0.2 mM and growth continued for 5 h at 24 °C under shaking. Cells were harvested by centrifugation at 4,000 × *g* for 10 min, resuspended in binding buffer (20 mM Tris-HCl, pH 7.5, 500 mM NaCl, 5 mM imidazole), and lysed by sonication on ice with a macroprobe sonicator (model XL2020, Misonix) at a power setting of 4 for 15 min. After centrifugation at 5000 rpm at 4 °C for 20 min, the supernatant was applied to a nickel-Sepharose column (GE Healthcare), and the chromatography was performed as recommended by the manufacturer. The eluting buffer consisted of 500 mM imidazole. The purity of the protein was then evaluated by SDS-PAGE.

Ion Pair HPLC Analysis of Nucleotide Sugars—This study used a Waters HPLC system (Waters 2796 Bioseparations Module) composed of an autosampler and a UV detector (Waters 2996 photodiode array detector) to analyze the amount of nucleotide sugars in cells. Separation of nucleotide sugars, NAD^+, and NADH was performed at 34 °C on a μBondapak C18 column (10-μm particle size, 3.9 × 300 mm) and a guard column cartridge (5-μm particle size, 4.6 × 20 mm, Atlantis®, Waters). The method was performed as described previously (19, 20). Two buffers were used for the HPLC analysis. Buffer A was 100 mM KH_2PO_4/K_2HPO_4 plus 8 mM tetrabutylammonium-bisulfate hydrogen sulfate used as the pairing reagent, pH 5.3. Buffer B was 70% buffer A plus 30% methanol, pH 5.9. Concentrate KOH or phosphoric acid was used for adjusting the buffer pH. All solutions were freshly prepared, filtered through a 0.2-μm filter (Millipore), and degassed before use. The sequence of chromatographic gradient was as follows: 100% buffer A for 2.5 min, 0–40% buffer B for 14 min, 40–100% buffer B for 1 min, 100% buffer B for 6 min, 100–100% buffer B for 1 min, followed by an equilibration phase of 100% buffer A for 8 min. The flow rate was 1.0 ml/min.

Enzymatic Activity and Kinetic Characterization—UGDH activity was measured by monitoring the change in absorbance at 340 nm, which accompanies the reduction of NAD^+ to NADH. The assay was performed at room temperature in 0.1 M Tris-HCl buffer, pH 7.5, containing 5 mM UDP-Glc, 1 mM dithiothreitol (DTT), 1 mM $MgCl_2$, and 5 mM NAD^+. One unit of UGDH activity is defined as the amount of enzyme required to produce 2 μmol of NADH per min at room temperature. Prior to HPLC analysis, the reaction mixture was mixed thoroughly with an equal volume of methanol, and the protein precipitate was removed by centrifugation at 20,000 × *g* for 30 min. The K_m and V_{max} values for UDP-Glc and NAD^+ were determined independently using standard assay conditions. Kinetic parameters for UDP-Glc as the substrate were measured by holding NAD^+ constant (5 mM) and varying UDP-Glc from 0.02 to 5 mM. Similarly, NAD^+ kinetic measurements were made by holding UDP-Glc constant (5 mM) and varying NAD^+ from 0.02 to 5 mM. GraphPad Prism4 software plotted the data, and K_m and V_{max} were calculated by fitting the data to the equation ($V = V_{max}[S]^h/([S]^h + K_m{}^h)$), where h is the Hill coefficient. Substrate specificity was measured by substituting UDP-Glc with the same concentration of ADP-Glc, TDP-Glc, GDP-Man, UDP-Gal, or UDP-GlcNAc in the standard reaction. To determine the K_i value of UDP-GlcUA, the K_m value of UDP-Glc at a variety of concentrations of UDP-GlcUA was first measured. The results were then fitted onto a curve where X is the concentration of UDP-GlcUA, and Y is the observed K_m value. Linear regression was used to determine the x axis intercept, which equals the negative K_i value. The measurement of K_i for NADH was carried out similarly in the presence of variable concentrations of the compound.

Molecular Mass Determination—The molecular masses of PA2022 and PA3559 in aqueous solution were determined using a Superdex-200 10/300 GL column (GE Healthcare) on a fast protein liquid chromatograph in 100 mM Tris-HCl, pH 7.5, containing 300 mM NaCl, at a flow rate of 0.5 ml/min. Size determination was made by comparing molecular mass standards (GE Healthcare) chromatographed under the same conditions. The molecular mass standards used were as follows: ferritin, 440 kDa; aldolase, 158 kDa; albumin, 67 kDa; RNase A, 15 kDa. A calibration curve was plotted as the log (molecular mass) *versus* K_{av}, where $K_{av} = (V_e - V_0)/(V_t - V_0)$, giving correlation values above 0.99. The term V_e is the elution volume for the protein; V_0 is the column void volume, and V_t is the column total bed volume. The molecular masses of PA2022 and PA3559 were subsequently determined from the calibration curve.

Construction of PA2022 and PA3559 Deletion Strains—Constructing the *PA3559* gene-specific deletion mutants in *P. aeruginosa* involved obtaining DNA fragments of ~1 kb in size both upstream and downstream of the targeted sequences to be deleted by PCR amplification of genomic DNA of *P. aeruginosa* PAO1. Primers pmrE05 and pmrE03 were used for amplifying upstream fragments, and primers pmrE04 and pmrE06 (Table 2) were used for the downstream region. The amplified fragments were then cloned in tandem into the suicide vector pEX18Tc. For *PA2022* mutant construction, a 4.1-kb DNA segment comprising the *PA2022* gene was first cloned into the PstI and EcoRI sites of the suicide vector pSUP202. The next step was to insert a kanamycin resistance gene in the unique BamHI site of the *PA2022* gene. In either case, the resulting gene replacement plasmids were transformed individually into *E. coli* SM10 and subsequently mobilized into *P. aeruginosa* PAO1 or its derivatives via conjugation. The transconjugants were selected on LB agar containing tetracycline (50 μg/ml) and ampicillin (100 μg/ml), which was used to counterselect donor *E. coli*. The surviving colonies were then propagated in LB broth containing 5% sucrose, which selected against cells containing the *sacB* gene harbored on pEX18Tc. These colonies were also tested for tetracycline sensitivity to ensure plasmid loss. The resultant mutants were confirmed by PCR amplification and Southern hybridization with a probe specific to each of the genes.

Preparation of the Cell-free Extracts for UGDH Activity Determination—The bacteria grown overnight were refreshed in 50 ml of LB broth for 2 h and collected by centrifugation. The pellet was resuspended in 30 ml of buffer containing 100 mM Tris-HCl, 20 mM NaCl, 1 mM $MgCl_2$, 1 mM DTT, 1 mM phen-

ylmethylsulfonyl fluoride, pH 7.5, disrupted by a brief ultrasonication, and centrifuged for 20 min at 14,000 × *g* to remove the debris. The clarified cell lysates were dialyzed overnight against 100 mM Tris-HCl, 1 mM $MgCl_2$, 1 mM DTT, pH 7.5, prior to determination of the UGDH activity. The cell lysate (~15 μg of protein) in this specific assay was first incubated with NAD^+ to determine the endogenous NAD^+ reduction rate. UDP-Glc was then added to the reaction mixture, and the difference in the NAD^+ reduction rate was measured. Here the definition of 1 unit is the activity that produces 1 μmol of NADH per min.

Extraction of Intracellular Nucleotide Sugars—Bacterial cells from the 0.5-ml overnight culture were collected by centrifugation. The pellet was briefly washed with phosphate-buffered saline, and 185 μl of a cold 0.5 M perchloric acid solution was added to the pellet and mixed vigorously. After incubation on ice for 2 min, the samples were centrifuged at 10,000 × *g* at 4 °C, for 5 min. The supernatants containing the soluble molecules were neutralized with 42 μl of ice-cold 2.5 M KOH in 1.5 M K_2HPO_4 and incubated on ice for 2 min. The neutralized samples were centrifuged again and filtered with 0.2-μm filters (Millipore, Billerica, MA) to remove potassium perchlorate precipitate. The samples were stored at −70 °C until analysis.

Susceptibility to Antibiotics—Antibiotic-impregnated disks (BBL™, Oxoid or Difco) were used to measure the sensitivity of the bacterial strains to antibiotics. For the disk diffusion assay, overnight aerobically grown cultures in LB were diluted to an A_{600} of 0.1, and 100-μl aliquots were spread uniformly on an LB plate. The disk loads were as follows: ampicillin, 10 μg; polymyxin B, 300 IU; ceftazidime, 30 μg; cefotaxime, 30 μg; chloramphenicol, 30 μg; gentamicin, 10 μg; imipenem, 10 μg; kanamycin, 30 μg; lincomycin, 2 μg; and tetracycline, 30 μg. Comparing the zone of inhibition to a standard sensitivity chart (BD Biosciences) revealed the resistance to an antibiotic. The MIC of each antibiotic was determined by the microdilution method in multiple-well plates. The MIC was defined as the lowest concentration of antibiotic that prevented growth of the testing bacterial strains after 18 h of incubation at 37 °C.

Bacterial Motility Assays—For swimming motility assays (21), tryptone swim plates (1% tryptone, 0.5% NaCl, 0.3% agar) were inoculated with a sterile toothpick and incubated for 12–14 h at 25 °C. Motility was then assessed qualitatively by examining the circular turbid zone formed by the bacterial cells migrating away from the point of inoculation. For the twitching motility assay, cells were stab-inoculated with a toothpick through a thin (~3 mm) LB agar layer (1% agar) to the bottom of the Petri dish. After incubation from 24 to 48 h at 37 °C, a hazy zone of growth at the interface between the agar and the polystyrene surface was revealed by crystal violet staining (1% (w/v) solution) (22).

LPS Analysis—The hot phenol-water method (23) and the proteinase K digestion method (24) were utilized to extract LPS. The LPS preparations were separated on a 12.5% SDS-polyacrylamide gel and silver-stained according to a previously published method (25).

Reverse Transcription and Real Time-PCR—Total RNA was isolated by using the High Pure RNA isolation kit (Roche Applied Science). Two micrograms of total RNA was reverse-transcribed in a 20-μl reaction mixture containing 50 units of Moloney murine leukemia virus reverse transcriptase, 5 μM DTT (both from Invitrogen), 40 units of RNaseOUT recombinant ribonuclease inhibitor (Promega) 0.5 μM of random hexanucleotide primers (GE Healthcare), and 500 μM of dNTP mixture. The reverse transcription reaction was carried out at 50 °C for 60 min. Heating the reaction mixture at 70 °C for 15 min was subsequently performed to terminate the reaction, and the cDNA was stored at −20 °C.

All real time PCR analyses were performed on an ABI PRIZM 7000 instrument. Each reaction included a 20-μl reaction mixture containing 0.1 μM of each primer, 10 μl of 2× SYBR Green PCR master mix (Applied Biosystem, including AmpliTaq Gold DNA polymerase with buffer, dNTPs mix, SYBR Green I dye, Rox dye, and 10 mM $MgCl_2$), and 1 μl of the template cDNA. The typical amplification program included activation of the enzyme at 94 °C for 10 min, followed by 40 cycles of denaturation at 94 °C for 15 s, and annealing and extension at 60 °C for 1 min. The C_T (cycle threshold) value for each gene was determined by automated threshold analysis function of the ABI instrument and normalized to $C_{T(\mathrm{G3PDH})}$ to obtain dC_T ($= C_{T(\mathrm{G3PDH})} - C_{T(\mathrm{test})}$). The difference in gene expression at different Mg^{2+} concentrations was indicated with the ddC_T values, which were calculated as $dC_{T(\mathrm{low\ Mg^{2+}})} - dC_{T(\mathrm{high\ Mg^{2+}})}$. The difference of n between two C_T or dC_T values indicates a 2^n-fold difference in amount of the target sequence between the two cDNA samples being compared.

Biofilm Assay—The kinetics of biofilm formation in a static system was measured as described by O'Toole and Kolter (26). Briefly, LB was inoculated with an overnight culture of each strain at a 1/100 dilution, and 100-μl aliquots of the diluted bacterial suspension were added to a 96-well polystyrene microtiter dish. The microtiter dish was incubated at 37 °C in a humidified chamber. The liquid culture was removed by aspiration, and the wells were rinsed thoroughly two times with phosphate-buffered saline at each time point. Samples were stained by adding 100 μl of 1% crystal violet solution to each well and allowing them to sit for 15 min. After staining, the wells were washed three times with water, and any remaining crystal violet in the wells was dissolved in 100 μl of 95% ethanol, and the absorbance at 595 nm was determined. Alternatively, the biofilm-forming capability of these strains was evaluated by using a polydimethylsiloxane flow cell connected to a bacterial culture system, which allowed the culture media flowing through the flow cells at uni-direction. Before perfusion, 10 ml of mid-log phase ($A_{600} = 0.5$) *P. aeruginosa* was injected into the microchannels by a polypropylene syringe. The flow cells were incubated for 1 h at 25 °C to allow initial bacteria attachment. A peristaltic pump then passed a 1:10 dilution of LB broth through the flow cell at a flow rate of 10 ml/min. After 24 h, the biofilms formed in the flow cell were labeled with SYBR Green solution for 5 min and then examined under a Zeiss LSM 510 laser-scanning confocal microscope. Optical sections with a step size of 3 μm in the *z* axis were collected and reconstructed into three-dimensional cross-sections.

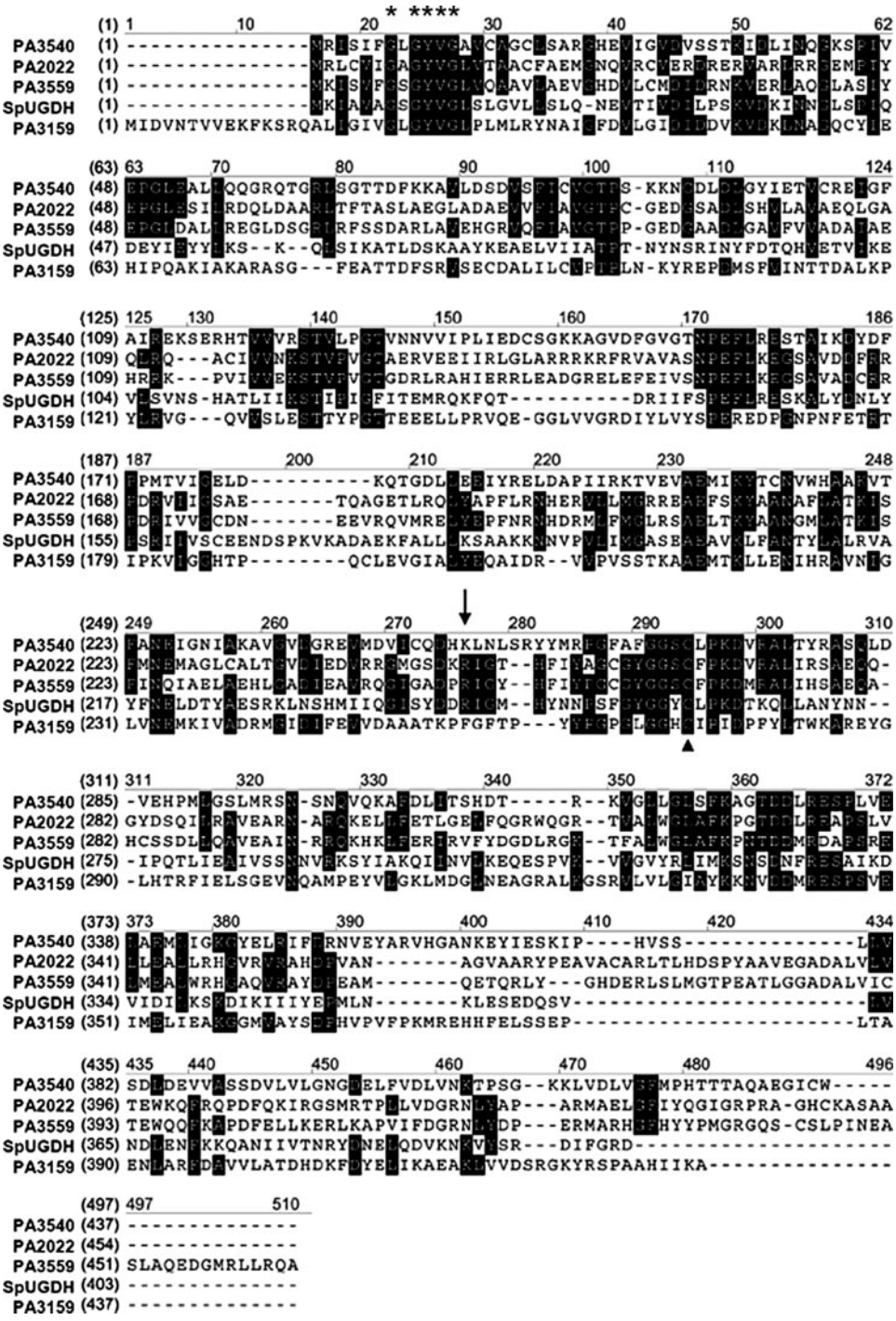

FIGURE 1. **Sequence comparison of UGDH homologs.** Multiple sequence alignment of *S. pyogenes* SpUGDH (GenBank™ accession number NP_270108), *P. aeruginosa* PA2022 (NP_250712), PA3559 (NP_252249), PA3540 (NP_252230), and PA3159 (NP_251849) is shown. The *asterisks* indicate the position of the Rossmann fold, which contains a consensus sequence G*X*G*XX*G. The *arrow* points to a residue that determines the substrate specificity of the enzymes. The *arrowhead* indicates the catalytic Cys-266 of PA2022, with a flanking sequence of GG*XCXXX*D. Residues identical in at least three of the comparison sequences are *highlighted*.

RESULTS

Identification of UGDH Homologs in P. aeruginosa PAO1 Genome—Because the *Streptococcus pyogenes* UGDH (SpUGDH) molecular structure was solved previously (27), the protein sequence was used as a template to search for UGDH homologs in *P. aeruginosa* PAO1. Four genes, *PA2022*, *PA3159*, *PA3540*, and *PA3559*, were capable of encoding a protein with a sequence identity ranging from 22 to 25% compared with that of SpUGDH. Among them, *PA3540* (*algD*) and *PA3159* (*wbpA*) have been characterized previously as GDP-Man dehydrogenase (GMDH) (28) and UDP-GlcNAc 6-dehydrogenase encoding gene, respectively (29), but *PA2022* and *PA3559* have not been investigated. Alignment of the putative protein sequences of these genes indicates that, in comparison with PA3540 and PA3159, PA2022 and PA3559 resemble SpUGDH with a BLASTP e value of 2×10^{-23} and 7×10^{-22}, respectively. PA3559 and PA2022 are closely related to each other and share 52% identity and 67% similarity. Both proteins contain a NAD^+ dinucleotide-binding domain in the N-terminal regions and a nucleotide sugar-binding domain in the C-terminal regions (Fig. 1). The signature of the NAD^+-binding domain, *i.e.* three glycines in the G*X*G*XX*G "fingerprint" of the Rossmann fold (30), was strictly conserved among these putative nucleotide sugar dehydrogenases. In addition, these two proteins also contain Cys-260 in SpUGDH and its flanking sequence GG*XCXXX*D, which is known to participate in catalysis. Finally, like the other UGDH, PA2022 and PA3559 both contain an Arg at a position corresponding to Arg-244 in SpUGDH. This Arg is thought to be one of the determinants of substrate specificity in nucleotide sugar dehydrogenases (27). This contrasts with GMDH and UDP-GlcNAc dehydrogenase, in which that position contained a Lys and a Phe, respectively (Fig. 1). Based on the highly conserved sequence features, this study hypothesizes that both PA2022 and PA3559 encode a nucleotide sugar dehydrogenase, and it is most likely a UGDH.

Oligomeric Structure of PA2022 and PA3559 Gene Products—The oligomeric structure of nucleotide sugar dehydrogenases varies considerably in different organisms. The *P. aeruginosa* UDP-GlcNAc dehydrogenase (WbpA) is a trimer (29), whereas SpUGDH is a monomer (27) in solutions. On the other hand, *E. coli* UGDH (32) and *P. aeruginosa* GMDH display a dimeric and a tetrameric form, respectively (33). Gel filtration chromatography reveals that the

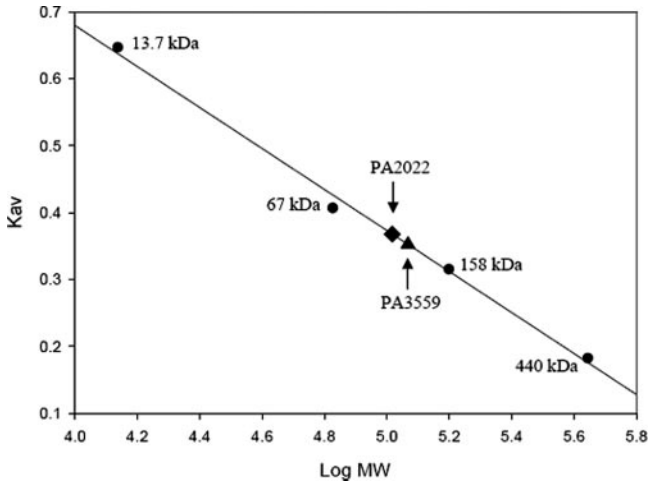

FIGURE 2. **Determination of the oligomeric states of PA2022 and PA3559.** Purified PA2022 and PA3559 were fractionated individually by gel filtration fast protein liquid chromatography on a Superdex 200 HR 10/30 column. The size was determined by comparing molecular weight standards resolved under the same conditions. The average retention time in the column was plotted *versus* the log of the molecular weight for each standard. The sizes of PA2022 and PA3559 are indicated with ♦ and ▲, respectively.

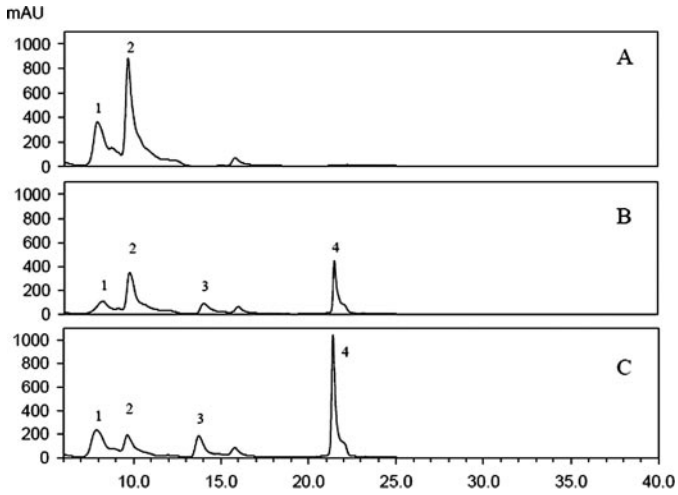

FIGURE 3. **Characterization of the reaction catalyzed by PA2022 and PA3559.** The standard UGDH assay was performed in the absence (*A*) or presence of the gene product of either PA2022 (*B*) or PA3559 (*C*). *Peak 1*, UDP-Glc; *peak 2*, NAD; *peak 3*, UDP-GlcUA; *peak4*, NADH. *mAU* is milliabsorption units at 260 nm.

native conformation of PA2022 and PA3559 is ~104 and 117 kDa, respectively (Fig. 2). Because the predicted mass of PA2022 and PA3559 is 54.5 and 57.4 kDa, respectively, both proteins are probably present in a dimeric form in native conditions, as also found for the *E. coli* UGDH.

Characterization of Enzymatic Activity in PA2022 and PA3559—Determining whether PA2022 and PA3559 exhibit UGDH activity was evaluated by incubating the enzyme with UDP-Glc and analyzing the reaction product via HPLC. Commercially available nucleotide sugars served as the references. The recombinant PA2022 and PA3559 were first produced in *E. coli* as a His_6-tagged protein and purified to near homogeneity as estimated by SDS-PAGE. Once purified, DTT and $MgCl_2$ were immediately added to the enzyme preparation, to a final concentration of 1 mM each, to maintain the enzyme activity. The conversion of UDP-Glc into UDP-GlcUA and NAD^+ into NADH by either PA2022 or PA3559 could be detected after incubating the enzyme in standard assay conditions for 30 min (Fig. 3). Thus, the HPLC assay demonstrates that both PA2022 and PA3559 are UGDH. The specificity of these two UGDHs to several other nucleotide sugars was further investigated by monitoring the rate of NADH synthesis in the reaction at 340 nm using a spectrophotometer. Using TDP-Glc, UDP-Gal, and UDP-GlcNAc as a substrate for PA2022 yielded a relative rate of 38.51, 6.37, and 34.95%, respectively, to the UDP-Glc rate (Table 3). PA3559 did not react with TDP-Glc and showed relatively low activity toward UDP-Gal and UDP-GlcNAc compared with PA2022. Therefore, PA3559 seems to possess higher substrate specificity than PA2022.

Determination of Kinetic Parameters of PA2022 and PA3559—The kinetic parameters of the UGDHs were determined by measuring NADH absorbance at 340 nm to detect the initial velocity of the reaction. The data were fitted to a modified Michaelis-Menten equation by nonlinear regression from $V = V_{max}[S]^h/([S]^h + K_m{}^h)$, and the kinetic parameters are listed in Table 4. Our result shows that PA2022 could utilize lower concentrations of both UDP-Glc and NAD^+ more efficiently than PA3559 as demonstrated by the smaller K_m values to these substrates (Table 4). In addition, the Hill plot of the UDP-Glc rate data revealed a Hill coefficient of 1.20 and 1.67 for PA2022 and PA3559, respectively. These numbers indicate that PA3559 exhibits slight allosteric effects for UDP-Glc kinetics. In addition, the initial reaction rate of PA3559 displays a clear lag when UDP-Glc was used as the substrate. This result contrasts with the PA2022 result, which reaches its maximal rate rapidly reflecting the distinct kinetic behaviors between these two enzymes (data not shown).

TABLE 3
Substrate specificity of PA2022 and PA3559
The specific activity of PA2022 and PA3559 used in the study was 0.52 and 0.23 units/mg, respectively.

Substrate	Relative activity[a]	
	PA2022	PA3559
	%	
UDP-Glc	100	100
ADP-Glc	ND[b]	ND
TDP-Glc	38.5	ND
UDP-Gal	6.4	11.9
GDP-Man	ND	ND
UDP-GlcNAc	35.0	6.3

[a] The initial reaction rate is relative to when UDP-Glc is used as the substrate. The concentration of all tested substrates was 5 mM.
[b] ND indicates not detected.

Effects of Reaction Product and Divalent Ions on the Enzyme Activity—Both NADH and UDP-GlcUA were used to investigate product inhibition effects on the reaction carried out by the two enzymes. The presence of UDP-GlcUA, the immediate product of the reaction catalyzed by UGDH, caused moderate inhibitions on the activity of both enzymes. The K_i values of UDP-GlcUA for PA2022 and PA3559 are 0.061 and 0.714 mM, respectively. The other reaction product, NADH, exhibits a relatively strong inhibition on both the enzyme activities. Compared with PA3559, PA2022 is more sensitive to NADH feedback inhibition and can be strongly affected by the compound even at 0.05 mM (Table 5). The K_i value of NADH, however, could not be determined accurately. Presumably, this is

TABLE 4

Kinetic parameters for PA2022 and PA3559

Parameters were determined by nonlinear regression from $V = V_{max}[S]^h/([S]^h + K_m{}^h)$.

		K_m	V_{max}	k_{cat}	k_{cat}/K_m	h
		mM	nmol × min^{-1}	min^{-1}	mM^{-1} × min^{-1}	
PA2022	UDP-Glc	0.12 ± 0.01	11.6 ± 0.5	14.4 ± 0.3	117.8 ± 2.5	1.20 ± 0.11
	NAD^+	0.47 ± 0.18	18.0 ± 2.6	22.4 ± 2.8	47.2 ± 2.7	1.35 ± 0.28
PA3559	UDP-Glc	0.40 ± 0.03	32.9 ± 2.0	48.4 ± 1.5	120.7 ± 3.7	1.67 ± 0.19
	NAD^+	1.99 ± 0.67	95.8 ± 12.0	141.0 ± 8.9	71.0 ± 4.5	0.84 ± 0.09

TABLE 5

Effects of reaction products and ions on PA2022 and PA3559 activity

Both UDP-Glc and NAD^+ concentrations used in the assays, with the exceptions in UDP-GlcUA and NADH inhibition studies, were 5.0 mM.

Treatment	Concentration	PA2022	PA3559
	mM	%	%
$MgCl_2$	1.0	100	100
$CaCl_2$	1.0	97 ± 3	84 ± 4
NaCl	1.0	99 ± 7	96 ± 3
$MnCl_2$	1.0	84 ± 12	92 ± 4
$MgSO_4$	1.0	100 ± 2	94 ± 3
Na_2SO_4	1.0	93 ± 8	98 ± 1
$(NH_4)_2SO_4$	1.0	98 ± 1	96 ± 2
EDTA	1.0	83 ± 4	98 ± 12
NADH[a]	0.05	26 ± 5	70 ± 5
NADH[a]	0.1	<1.0	59 ± 6
UDP-GlcUA[b]	0.5	57 ± 0.02	90 ± 2
UDP-GlcUA[b]	1.0	44 ± 0.01	79 ± 6

[a] The reaction rate was measured at 5.0 mM UDP-Glc and 1.0 mM NAD^+ and compared with that at the same condition without NADH.

[b] The reaction rate was determined at 0.5 mM UDP-Glc and 5.0 mM NAD^+ and compared with that at the same condition without UDP-GlcUA.

because of its strong absorption at 340 nm, which makes the analysis less accurate. These results suggest that the synthesis of UDP-GlcUA in *P. aeruginosa* is under tightly controlled and depends on the cellular NADH concentrations. Several divalent ions, including Mn^{2+}, Ca^{2+}, SO_4^{2-}, and chelator EDTA, were tested, but none of them showed significant activation or inhibition effects on the activity of both enzymes (Table 5).

Characterization of PA2022 and PA3559 Mutants of P. aeruginosa PAO1—Three gene-specific deletion strains in PAO1, RJ101 (ΔPA2022), RJ102 (ΔPA3559), and RJ103 (ΔPA2022, ΔPA3559), were constructed using the allelic exchange strategy to determine the functional roles of the two UGDHs in *P. aeruginosa* physiology. The correctness of the deletions was confirmed by PCR using the genomic DNA extracted from the strains as a template (supplemental Fig. S1). Real time quantitative PCR also verified the absence of corresponding mRNA in the mutant stains. The UGDH activity in the crude cell extract of these mutants was then determined and compared with UGDH activity in the parental strain. Our results revealed that under standard growth and assay conditions (see "Experimental Procedures"), the UGDH activity in the double deletion mutant RJ103 was clearly reduced, yielding a specific activity of 6.7 ± 0.4 units/mg of protein compared with 13.7 ± 0.7 units/mg of protein in the wild type PAO1. The enzyme activity in RJ101 and RJ102 also fell moderately to 9.4 ± 0.6 and 11.7 ± 0.9 units/mg of protein, respectively. The low UGDH activity remaining in the double deletion mutant RJ103 suggests that other nucleotide sugar dehydrogenases may also function as UGDH.

Nucleotide Sugar Profiling of PAO1 and UGDH Mutant Strains—Whether the cellular nucleotide sugar pool is affected in the UGDH mutants was unclear. Presumably, the accumulation of UDP-Glc and the absence of UDP-GlcUA would be observed in the UGDH mutants, in particular the double deletion mutant RJ103. Nevertheless, reverse-phase ion pair HPLC analysis of the cell extract indicates that UDP-Glc (retention time = 8.63 min) seems to remain at a constant level in all the strains. On the other hand, UDP-GlcUA could not be detected in any of the extracts, suggesting that the compound turnover rate is rapid in the bacterial cells. The metabolite profile of RJ101 is similar to that of RJ103, showing an additional peak compared with wild type PAO1. The extra peak eluted at a time point very close to UDP-Gal, suggesting that any extra UDP-Glc in RJ101 and RJ103 was partially converted to UDP-Gal (supplemental Fig. S3). Finally, the total uronic acid content amount in the EPS in each strain was examined. Contrary to expectations that the uronic acid content would be reduced because of the UGDH deficiency, all UGDH mutant strains synthesized a higher quantity of uronic acid than the wild type PAO1 (Table 6). A possible explanation for this finding is that GlcUA accounts for only a minor fraction of the uronic acid pool in *P. aeruginosa* cells, and the UDP-Glc that accumulated because of UGDH deficiency is re-directed to pathways for the synthesis of other uronic acids such as ManUA or GlcNAcUA.

Expression Levels of PA2022 and PA3559 in Response to Low Concentrations of Mg^{2+}—In *Salmonella enterica* serovar Typhimurium, the two-component system response regulator PmrA can activate UGDH gene expression when the cells are propagated in low Mg^{2+} concentrations. To test whether the expression of *PA2022* and *PA3559* can also be activated in low Mg^{2+}, a real time quantitative PCR experiment was performed to measure the expression level of these two genes. Our experimental data show that *PA2022* was constitutively expressed regardless of the concentration of Mg^{2+} in the medium (Fig. 4). In contrast, *PA3559* expression was activated in response to low Mg^{2+} with a 32-fold increase compared with high Mg^{2+} conditions (2.0 mM). This result strongly supports the hypothesis that *PA2022* and *PA3559* are regulated differently and respond to different environmental cues.

Susceptibility of the UGDH Mutants to Antibiotics—*P. aeruginosa* is notorious for its natural resistance to many antibiotics partly because of the permeability barrier afforded by its cell surface components. As UGDH normally plays an important role in LPS and EPS biosynthesis, it would be interesting to know if there is any difference in antibiotic susceptibility between the UGDH-deficient mutants and the wild type PAO1. An antibiotic sensitivity assay was performed by the standard disk diffusion assay. As Table 7 demonstrates, the susceptibility

of *PA2022* and *PA3559* mutants to polymyxin B, lincomycin, ampicillin, and kanamycin showed no significant differences from the wild type PAO1 when tested on LB plates. Interestingly, the mutants RJ101 and RJ103 were more susceptible to chloramphenicol and cefotaxime but not RJ102. Testing the MIC of each of the antibiotics to these bacterial strains further verified the findings. Two different Mg^{2+} concentrations were also tested to differentiate the possible roles of the two UGDH in antibiotic resistance. Our results indicate that RJ101 and RJ103 are indeed more susceptible than wild type PAO1 and RJ102 to ampicillin, chloramphenicol, and cefotaxime in either high (2.0 mM) or low concentrations of Mg^{2+} (0.02 mM) medium, although high concentrations produce a more pronounced effect (Table 8). On the other hand, RJ102 and RJ103 were more sensitive to polymyxin B when grown in low Mg^{2+} conditions, but not RJ101, implying that PA3559 is responsible for the polymyxin B resistance.

TABLE 6

Total uronic acid in *P. aeruginosa* PAO1 and *UGDH* mutants

Standard deviations for three measurements are shown.

Strains	Uronic acid
	μg/μg total protein
PAO1	0.36 ± 0.05
RJ101	0.60 ± 0.02
RJ102	0.60 ± 0.01
RJ103	0.59 ± 0.02

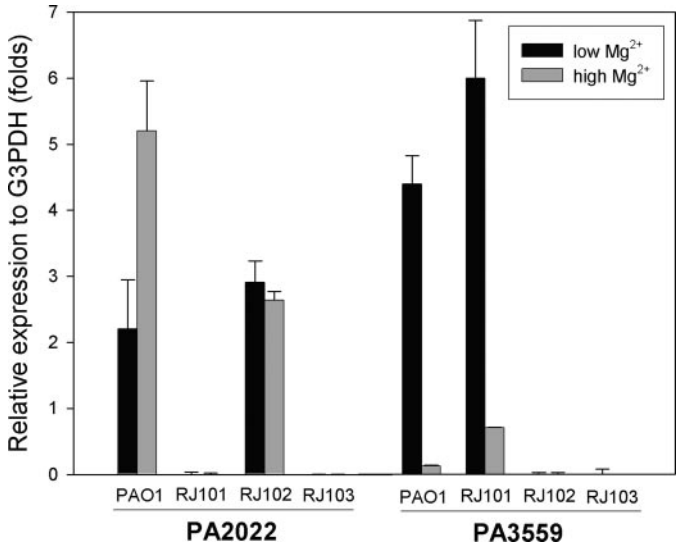

FIGURE 4. **Analysis of *PA2022* and *PA3559* gene expression by reverse transcription-quantitative PCR.** Wild type PAO1 was cultured in basal medium containing either 0.02 or 2.0 mM Mg^{2+}. The *PA2022* and *PA3559* gene expressions were determined as folds of G3PDH expression. The results are the average of three independent experiments.

Effects of UGDH Mutations on the Bacterial Biofilm Formation—Another mechanism producing drug resistance in *P. aeruginosa* is that the bacterium tends to colonize on solid surfaces, forming a biofilm that renders cells impervious to therapeutic concentrations of antibiotics. The biofilm formation capability of these UGDH mutant strains was examined by using the microtiter dish assay. As illustrated in Fig. 5, the parental strains PAO1, RJ101, and RJ102 showed similar levels of biofilm formation. The double mutant, RJ103, produced substantially smaller amounts of biofilm in microtiter dish wells than the other strains. All of the strains displayed similar growth rates indicating that the deficiency in biofilm formation in RJ103 was not the result of slow growth. Biofilm formation dynamics were also measured using nonagitated 96-well polystyrene microtiter dishes and in flow cells over a period of 3 days. The RJ103 strain apparently produced as much biofilm as PAO1 after an 8-h incubation, but the quantity of biofilm produced by this double UGDH mutant dropped at a faster rate than the other tested strains thereafter (Fig. 5). Confocal microscopy revealed that the biofilm formed by RJ103 appeared to be thinner and than that for wild type PAO1 (Fig. 6).

Effects of UGDH on Bacterial Motility—Bacterial motility has been shown to closely associate with biofilm formation. For instance, flagella participate in the initial stages of *P. aeruginosa* biofilm development. Type IV pilus-mediated twitching motility is also involved in biofilm formation (19), particularly when microcolonies grow to mature mushroom-like structures on a glass surface (14). Determining whether the UGDH mutant strains had a defect in either swimming or twitching motility might explain the

TABLE 7

Antibiotic susceptibilities of *P. aeruginosa* PAO1 and the *UGDH* mutants

The abbreviations used are as follows: CHL, chloramphenicol; CTX, cefotaxime; PMB, polymyxin B; CAZ, ceftazidime; LIN, lincomycin; AMP, ampicillin; KAN, kanamycin.

Strain	Zone of inhibition						
	CHL	CTX	PMB	CAZ	LIN	AMP	KAN
				mm			
PAO1	6	6	15.2	23.5	6	6	6
RJ101	15.5	11.7	15.2	27.2	6	6	6
RJ102	6	6	15.0	25.5	6	6	6
RJ103	13.5	9.0	14.5	28.0	6	6	6

TABLE 8

Effects of Mg^{2+} concentrations on MICs (μg/ml) of antibiotics in *P. aeruginosa* PAO1 and the *UGDH* mutants

The abbreviations used are as follows: CHL, chloramphenicol; CTX, cefotaxime; PMB, polymyxin B; AMP, ampicillin; KAN, kanamycin; LM, low Mg^{2+} concentration (0.02 mM); HM, high Mg^{2+} concentration (2.0 mM).

Strain	AMP		CTX		CHL		PMB	
	LM	HM	LM	HM	LM	HM	LM	HM
PAO1	400	1600	30	60	30	240	32	4.0
RJ101	200	200	7.5	7.5	7.5	30	32	4.0
RJ102	400	1600	30	60	15	240	2.0	4.0
RJ103	200	200	7.5	7.5	7.5	30	2.0	4.0

abnormal biofilm development. None of the strains exhibited significant differences in swimming or twitching motility.

Multiple UGDH Homologs in Pseudomonas sp.—The presence of two UGDH genes in *P. aeruginosa* PAO1 is most likely advantageous to the bacterium when confronting environmental changes. This finding prompted investigation of whether other *Pseudomonas* species also possess multiple copies of UGDH genes. Using *PA2022* and *PA3559* as templates to search homologous genes in the genome of 11 *Pseudomonas* species revealed that all of the tested genomes, including *P. aeruginosa, P. fluorescens, P. putida,* and *P. syringae,* harbored multiple copies of UGDH homologous gene (Table 9). Phylogenetic tree analysis indicates that these UGDH-like genes can be divided into four clades as follows: one is very similar to *PA2022*, another group resembles *PA3559*, one group contains UDP-GlcNAc dehydrogenase encoding genes, and the rest are more closely related to GMDH. We would like to note that *PA2022*-like genes only occur in *P. aeruginosa,* whereas *PA3559* orthologs are widely distributed in all *Pseudomonas* sp. (Fig. 7). In addition, *PA2022* is closely linked to the *galU* gene that encodes UDP-Glc pyrophosphorylase, an enzyme that synthesizes UDP-Glc. In comparison, no UGDH-like gene can be found near the *galU* and *gor*, which encodes a glutathione reductase, in other *Pseudomonas* species. On the other hand, all *PA3559*-like genes in *Pseudomonas* species, except for *P. putida,* are adjacent to the 7-gene polymyxin resistance (*pmr*) gene cluster. These genes are designated PA3552–3558 in PAO1 and have been annotated to encode enzymes for polysaccharide synthesis (34). Phylogenetic analysis suggests that *PA2022*, a unique member of UGDH gene family only found in *P. aeruginosa*, may be evolved from *PA3559* by gene duplication to adapt to environmental changes. The distinct biochemical properties and gene expression profiles of PA2022 and PA3559 support this notion.

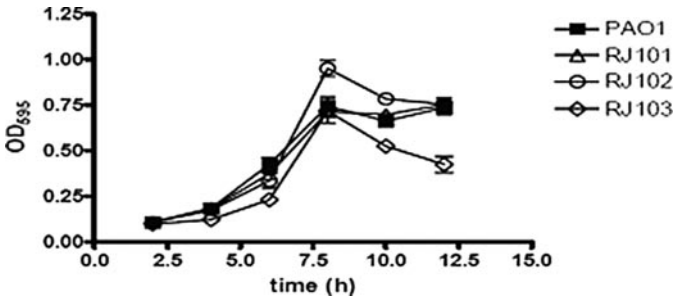

FIGURE 5. **Kinetics of biofilm formation in *P. aeruginosa* PAO1 and UGDH mutants.** The parental and mutant strains were grown in static culture in microtiter dishes. Biofilm formation kinetics was analyzed at different time points. The data are the means from two independent experiments, with each sample assayed in triplicate.

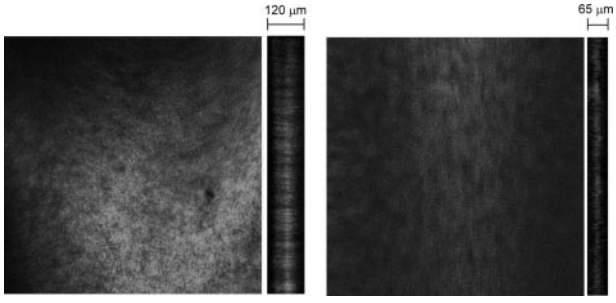

FIGURE 6. **Micrographs of the biofilm formed by the wild type PAO1 and the double mutant RJ103.** The tested bacteria were grown in a flow cell culture system and labeled by SYBR Green. Photographs were taken after 24 h of incubation using a laser-scanning confocal microscope at ×100 magnification with scans taken through the *z* axis to obtain 3-μm optical sections. The *panels above* and to the *right* of each top-down micrograph show side view micrographs of axis reconstructions.

DISCUSSION

This study presents evidence showing that both *PA2022* and *PA3559* encode a product with UGDH activity. Nevertheless, their biochemical properties as well as gene expression profiles are rather distinct. The fact that the PA2022 is the more efficient UGDH and is also constitutively expressed leads to the hypothesis that it is a housekeeping enzyme, responsible for converting most UDP-Glc to UDP-GlcUA in regular growth conditions. On the other hand, *PA3559* is expressed primarily under low Mg^{2+} stresses. This finding, together with its relatively large K_m value, implies that the PA3559 serves as a backup UGDH that functions only when the bacterium encounters unusual circumstances. These circumstances would include low concentrations of Mg^{2+} inside the phagosomes of a macrophage and whenever a large amount of UDP-Glc is available. In this regard, *PA3559* behaves more like the *Salmonella* UGDH gene whose expression is also activated in low Mg^{2+}. The UGDH is important in LPS and EPS modification and renders the bacteria resistant to antimicrobial peptides and phagocytes.

The three-dimensional molecular structure of SpUGDH was solved and reported by Campbell *et al.* (27). Subsequently

TABLE 9
Number of UGDH orthologs in *Pseudomonas* species

Strains	No. *UGDH*-like genes	Accession or gene index number
P. aeruginosa PAO1	4	PA2022, PA3559, PA3540, PA3159
P. aeruginosa UCBPP-PA14	4	PA14 38360,[a] PA14 18300,[b] PA14 18580,[c] PA14 23380
P. aeruginosa PA7[d]	3	ZP_01296258,[a] ZP_01295145,[b] ZP_01295164[c]
P. aeruginosa C3719[d]	2	ZP_00969565,[a] ZP_00968074[b]
P. fluorescens PfO-1	5	Pfl_2848,[b] Pfl_4070,[b] Pfl_2817,[b] Pfl_2024,[b] Pfl_0960[c]
P. fluorescens Pf-5	3	PFL3050,[b] PFL3078,[b] PFL1024[c]
P. putida KT2440	2	PP2926,[b] PP1288[c]
P. putida F1[d]	2	ZP_00900139,[b] ZP_00900762[c]
P. syringae pv. *syringae* B728a	3	Psyr2696,[b] Psyr5105,[b] Psyr1063[c]
P. syringae pv. *tomato* str. DC3000	3	PSPTO2891,[b] PSPTO5585,[b] PSPTO1243[c]
P. syringae pv. *phaseolicola* 1448A	2	PSPPH2809,[b] PSPPH1118[c]

[a] The sequence is more related to PA2022.
[b] The sequence is more related to PA3559.
[c] The sequence is more related to PA3540.
[d] The genome sequence was unfinished.

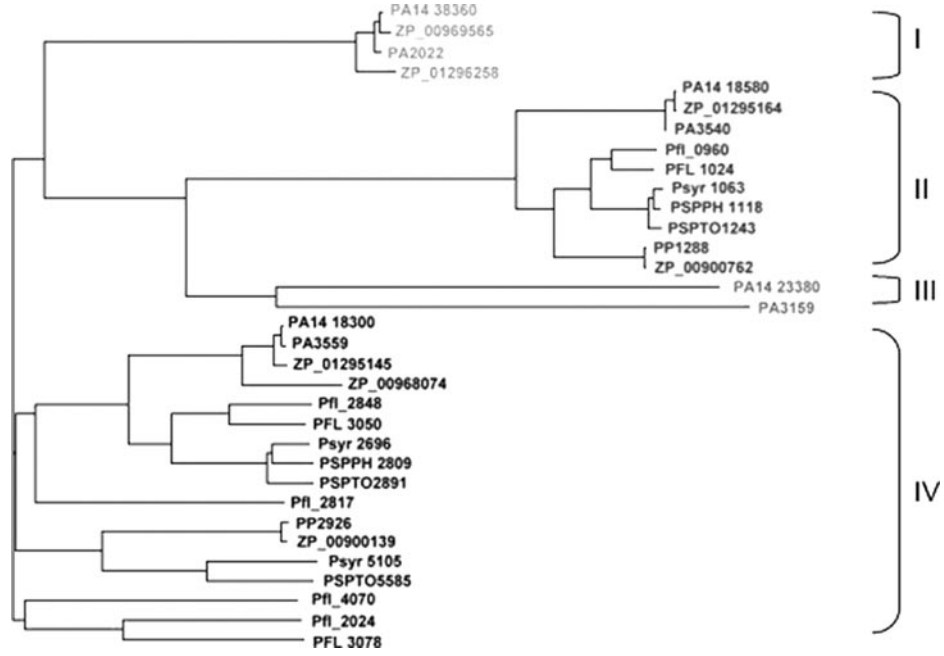

FIGURE 7. **Phylogenetic analysis of UGDH-like genes from several *Pseudomonas* species.** The genes were grouped into four families as follows: *PA2022*-like UGDH (*I*), GMDH (*II*), UDP-GlcNAc DHase (*III*), and *PA3559*-like UGDH (*IV*). The following prefixes indicate the species: *PA 14*, *P. aeruginosa* PA14; *Pfl_*, *P. fluorescens* PfO-1; *PFL*, *P. fluorescens* Pf-5; *PP*, *P. putida* KT2440; *Psyr*, *P. syringae* pv. *syringae* B728a; *PSPPH*, *P. syringae* pv. *phaseolicola* 1448A; *PSPTO*, *P. syringae* pv. *tomato* str. DC3000.

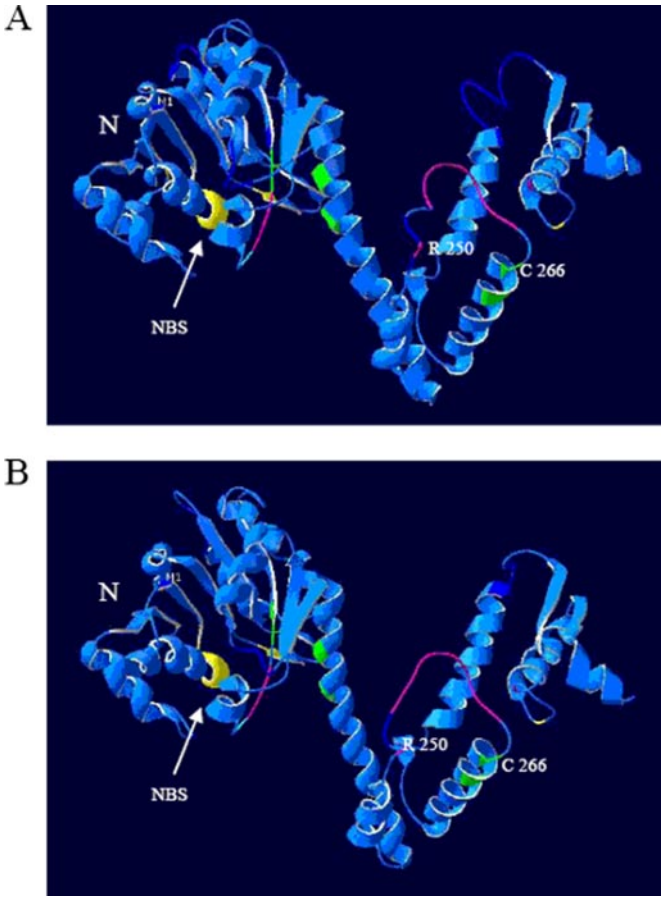

FIGURE 8. **The PA2022 and PA3559 structure models.** The N terminus, NAD-binding site (*NBS, yellow region*), UDP-Glc-binding site (*magenta loops*), and the catalytic site (*green regions*) containing Arg-250 and Cys-266 in PA2022 (*A*) and PA3559 (*B*) are indicated.

Snook *et al.* (33) determined the structure of a related enzyme, GMDH of *P. aeruginosa* PAO1. Using these structures as the template, the PA2022 and PA3559 structure predictions were performed at the Swiss-Model, and Fig. 8 shows the results. The structure model did not include C-terminal 100 amino acids because the high diversity of this region failed to fit proper templates. Overall, the structures of the two gene products resemble *P. aeruginosa* GMDH more than SpUGDH. The NAD^+ and UDP-Glc binding sites and catalytic sites of PA2022 and PA3559 were identified by comparing highly conserved SpUGDH domains and are indicated in Fig. 8, *A* and *B*. Both proteins contain a NAD^+ dinucleotide-binding domain in the N terminus and a nucleotide sugar-binding domain in the C-terminal regions, which are interconnected with a long (33 residues) α-helix. Superimposing PA2022 and PA3559 reveals that both main structures are highly similar except for some flexible loops. Cys-266 in PA2022 and PA3559 is at a position equivalent to the catalytic nucleophile Cys-260 in SpUGDH. The distance between the UDP-Glc-binding site and the catalytic site is too great for the reaction occurring in a single protein molecule. Therefore, this study proposes that the enzymes become active only when they form domain-swapped dimers that place the N-terminal domain of one monomer in close association with the C-terminal domain of the adjacent monomer. However, this speculation must be tested experimentally.

An intriguing question is the fate of UDP-GlcUA in *P. aeruginosa* PAO1. Many cystic fibrosis *P. aeruginosa* strains produce exopolysaccharide alignate, which does not rely on UGDH activity. However, it is not clear whether these strains could also produce another type of EPS containing GlcUA or its derivative. Similarly, the composition of EPS in noncystic fibrosis clinical *P. aeruginosa* isolate is also not clear. Some early studies demonstrated that certain *P. aeruginosa* strains produce a polysaccharide that could be degraded by hyaluronidase (35, 36). Another study found that HA accounts for as much as 7% of the biofilm slime materials in a *P. aeruginosa* strain (37). HA is a polysaccharide consisting of alternative GlcUA and GlcNAc residues. The UDP-GlcUA synthesized by PA2022 and PA3559 might therefore contribute to HA synthesis in *P. aeruginosa* PAO1, because PAO1 also has a GlcNAc synthesis pathway according to the Kyoto Encyclopedia of Genes and Genomes data base analysis. Consistent with this notion, data from the current study show that RJ103, a *PA2022-PA3559* double mutant, produces thinner biofilm than the wild type PAO1. Taken together, this information strongly suggests that the functional role of UGDH in *P. aeruginosa* at least partly involves

HA synthesis, which also contributes to biofilm formation. In addition, HA enables bacteria to evade the immune system of a host because of its nonimmunogenic nature. In most bacteria, there can be an overlap between EPS and LPS synthesis gene functions (37). Examining the LPS composition of UGDH mutant strains and the wild type PAO1 addresses this question and shows that they are indistinguishable on a silver-stained SDS-polyacrylamide gel.

This study provides direct evidence showing that UGDH is associated with antibiotic resistance in *P. aeruginosa*. In addition, PA2022 and PA3559 appear to play a distinct role in the phenomenon. The strains RJ101 and RJ103, in which *PA2022* is deleted, are more susceptible to chloramphenicol and cefotaxime (Table 8) in both high and low Mg^{2+} conditions. This susceptibility reflects on the housekeeping role of PA2022. Because these antibiotics are distinct in their chemical structure and mode of action, changes in susceptibility to these antibiotics are most likely because of a nonspecific mechanism such as alterations in bacterial membrane permeability that modulate antibiotic entry into the cell. On the other hand, deleting *PA3559* in *P. aeruginosa* caused a decrease in resistance levels to polymyxin B when propagated in low Mg^{2+} medium. Presumably, this effect is because of the higher expression levels of *PA3559* in the growth conditions. Thus, *PA3559* is likely to behave like its orthologous gene in the *S. enterica* serovar Typhimurium. The *Salmonella* UGDH gene participates in the pathway for synthesizing 4-amino-4-deoxy-L-arabinose, which affects lipid-A modification and produces polymyxin resistance (38). Nevertheless, other possibilities cannot be ruled out. For instance, the enzyme may modify or metabolize antibiotics directly, although we are not aware of any related finding being reported before.

Because of its critical role in EPS synthesis, UGDH has been considered as a crucial drug target (27). The presence of multiple UGDHs in *Pseudomonas* species makes this idea seem less attractive, however. Nevertheless, as a deficiency in UGDH could produce higher drug susceptibility in *P. aeruginosa*, a UGDH inhibitor may be used in combination with a clinically available antibiotic, as exemplified in the β-lactam drugs/β-lactamase inhibitor. Further investigation on how UGDH affects drug susceptibility in bacteria may reveal new implications for future drug development.

REFERENCES

1. Seifert, G. J. (2004) *Curr. Opin. Plant Biol.* **7,** 277–284
2. Princivalle, M., and de Agostini, A. (2002) *Int. J. Dev. Biol.* **46,** 267–278
3. Hauser, S. C., Ziurys, J. C., and Gollan, J. L. (1984) *J. Biol. Chem.* **259,** 4527–4533
4. Dalessandro, G., and Northcote, D. H. (1977) *Biochem. J.* **162,** 281–288
5. Roden, L. (1980) *The Biochemistry of Glycoproteins and Proteoglycans*, Plenum Publishing Corp., New York
6. Binari, R. C., Staveley, B. E., Johnson, W. A., Godavarti, R., Sasisekharan, R., and Manoukian, A. S. (1997) *Development* (*Camb.*) **124,** 2623–2632
7. Hacker, U., Lin, X., and Perrimon, N. (1997) *Development* (*Camb.*) **124,** 3565–3573
8. Haerry, T. E., Heslip, T. R., Marsh, J. L., and O'Connor, M. B. (1997) *Development* (*Camb.*) **124,** 3055–3064
9. Garcia-Garcia, M. J., and Anderson, K. V. (2003) *Cell* **114,** 727–737
10. Watson, D. A., and Musher, D. M. (1990) *Infect. Immun.* **58,** 3135–3138
11. Wessels, M. R., Goldberg, J. B., Moses, A. E., and DiCesare, T. J. (1994) *Infect. Immun.* **62,** 433–441
12. Cross, A. S. (1990) *Curr. Top. Microbiol. Immunol.* **150,** 87–95
13. Moxon, E. R., and Kroll, J. S. (1990) *Curr. Top. Microbiol. Immunol.* **150,** 65–85
14. Crater, D. L., and van de Rijn, I. (1995) *J. Biol. Chem.* **270,** 18452–18458
15. Griffith, C. L., Klutts, J. S., Zhang, L., Levery, S. B., and Doering, T. L. (2004) *J. Biol. Chem.* **279,** 51669–51676
16. Rocchetta, H. L., Burrows, L. L., and Lam, J. S. (1999) *Microbiol. Mol. Biol. Rev.* **63,** 523–553
17. Rajan, S., and Saiman, L. (2002) *Semin. Respir. Infect.* **17,** 47–56
18. Sambrook, J., and Russell, D. W. (2001) *Molecular Cloning: A Laboratory Manual*, 3 Ed., Cold Spring Harbor Laboratory Press, Cold Spring Harbor, NY
19. Ryll, T., and Wagner, R. (1991) *J. Chromatogr.* **570,** 77–88
20. Kochanowski, N., Blanchard, F., Cacan, R., Chirat, F., Guedon, E., Marc, A., and Goergen, J. L. (2006) *Anal. Biochem.* **348,** 243–251
21. Rashid, M. H., and Kornberg, A. (2000) *Proc. Natl. Acad. Sci. U. S. A.* **97,** 4885–4890
22. Darzins, A. (1993) *J. Bacteriol.* **175,** 5934–5944
23. Apicella, M. A., Griffiss, J. M., and Schneider, H. (1994) *Methods Enzymol.* **235,** 242–252
24. Hitchcock, P. J., and Brown, T. M. (1983) *J. Bacteriol.* **154,** 269–277
25. Fomsgaard, A., Freudenberg, M. A., and Galanos, C. (1990) *J. Clin. Microbiol.* **28,** 2627–2631
26. O'Toole, G. A., and Kolter, R. (1998) *Mol. Microbiol.* **30,** 295–304
27. Campbell, R. E., Mosimann, S. C., van De Rijn, I., Tanner, M. E., and Strynadka, N. C. (2000) *Biochemistry* **39,** 7012–7023
28. Deretic, V., Gill, J. F., and Chakrabarty, A. M. (1987) *Nucleic Acids Res.* **15,** 4567–4581
29. Miller, W. L., Wenzel, C. Q., Daniels, C., Larocque, S., Brisson, J. R., and Lam, J. S. (2004) *J. Biol. Chem.* **279,** 37551–37558
30. Rossman, M. G. (1981) *Philos. Trans. R. Soc. Lond. B. Biol. Sci.* **293,** 191–203
31. Hoang, T. T., Karkhoff-Schweizer, R. R., Kutchma, A. J., and Schweizer, H. P. (1998) *Gene* (*Amst.*) **212,** 77–86
32. Schiller, J. G., Bowser, A. M., and Feingold, D. S. (1973) *Biochim. Biophys. Acta* **293,** 1–10
33. Snook, C. F., Tipton, P. A., and Beamer, L. J. (2003) *Biochemistry* **42,** 4658–4668
34. McPhee, J. B., Bains, M., Winsor, G., Lewenza, S., Kwasnicka, A., Brazas, M. D., Brinkman, F. S., and Hancock, R. E. (2006) *J. Bacteriol.* **188,** 3995–4006
35. Warren, G. H., and Gray, J. (1954) *J. Bacteriol.* **67,** 167–170
36. Warren, G. H., and Gray, J. (1955) *J. Bacteriol.* **70,** 152–157
37. Brown, M. R., Foster, J. H., and Clamp, J. R. (1969) *Biochem. J.* **112,** 521–525
38. Gatzeva-Topalova, P. Z., May, A. P., and Sousa, M. C. (2005) *Structure* (*Lond.*) **13,** 929–942
39. Hughes, J. E., Stewart, J., Barclay, G. R., and Govan, J. R. (1997) *Infect. Immun.* **65,** 4281–4287
40. Simon, R., Priefer, U., and Pühler, A. (1983) *Bio/Technology* **1,** 784–791